

Detection of Distributed Sources Using Sensor Arrays

Yuanwei Jin, *Member, IEEE*, and Benjamin Friedlander, *Fellow, IEEE*

Abstract—In this paper, we consider the problem of detecting a random spatially distributed signal source by an array of sensors. We start with an approximate likelihood ratio (LR) detector and analyze its performance. Using the generalized likelihood ratio (GLR) approach, we then derive detectors under several assumptions on the available statistics. The performance of these detectors is evaluated, and the effect of the angular spread of the source is investigated. The detection performance behaves differently under different scenarios. We notice that the degrees of freedom (DOF) of the distributions of the detection statistics depend on both the signal angular spread and the number of data snapshots. Specifically, at a high SNR level and with small degrees of freedom, an increase of angular spread improves the detection performance. However, with large degrees of freedom, the increase of angular spread reduces detection performance. We provide a detailed discussion of the behavior of detection performance under various conditions. A comparison between the GLR detectors and conventional beamformer detectors is made by computer simulations. The results indicate that the GLR detectors perform better as the angular spread becomes large than that of the conventional beamformer detectors.

Index Terms—Detection, distributed source, generalized likelihood ratio (GLR), sensor array.

I. INTRODUCTION

A LARGE class of modern array processing techniques are designed for point sources, i.e., spatially discrete sources of acoustic or electromagnetic energy. In many practical situations, the transmitter is best modeled as a distributed, rather than a point source. The distributed sources appear to have certain angular spread with a mean direction of arrival (DOA). The point source model is only an approximation of the practical situation when there is a large distance between the source and the receiver array. The principal mechanism for making the source appear to be distributed in space is diffuse (unresolvable) and specular (resolvable) multipath caused by scattering of the propagating waves. For instance, experimental results obtained in urban wireless communications reported significant angular scattering distributions due to local scattering and reflection from mobile stations [2], [10], [12] and base stations [7], [17]. The characterization of the power azimuth spectrum shows that angular spreads as large as 25° have been observed. The amount of angular spread is highly dependent of the scattering around the mobile, the height of the base station, and the distance between the base station and the mobile station. A sec-

ondary, but equally important, mechanism is transmitter motion. If the source moves significantly during the observation interval (or coherent integration time), it will appear to be distributed rather than discrete. This is a typical scenario in sonar application where large number of sensors are used to obtain narrow beams. The moving acoustic sources may travel across several beams during an observation time [6]. Angular spread has a significant impact on any array processing algorithms [20]. For instance, the signal to noise ratio gain (SNRG) of the array reduces as the angular spread increases [8], causing possible performance degradation.

In passive array signal processing area, the problems under study concern the extraction of information from measurements using an array of sensors. Given the observations of the sensor outputs, the objective is to estimate the unknown parameters associated with the waveforms corrupted by noise. To this end, we start with a simple and computationally efficient detection scheme. If the “noise only” hypothesis is rejected, other algorithms are used to estimate the number of the sources and their unknown parameters, such as range and bearing.

Prior work on distributed sources focuses primarily on source localization and DOA estimation (see, e.g., [1], [4], [19], and [23]). Estimation of the number of distributed sources has also been studied in [1]. Subspace detectors have been studied in [18] and [21] for the cases where the signal lies in a deterministic subspace. More recently, the case of detecting Gaussian signals with a low-rank covariance matrix is studied in [15], and matched subspace detectors are developed based on the generalized likelihood ratio (GLR) principle.

In both cases, the subspace in which the signals lie is assumed to be known; in other words, the dimension and rank of the signal subspace are assumed to be known *a priori*. However, this assumption does not hold in practical situations. The rank, orientation, and strength of the signal subspace vary along with the signal angular spread, DOA, and the energy distribution function. In this case, the unknown parameters may be estimated based on the maximum likelihood principle.

In this paper, we develop detectors for distributed sources and study their performance, which is dependent of the angular spread. We first look at the case where all the parameters are known. In this case, the likelihood ratio detector can be approximated as a subspace beamformer. The detection performance depends on the distribution of the detection statistics and the sensor SNR. The degrees of freedom (DOF) of the detection statistics are determined by the angular spread and the number of data snapshots. If we fix the number of data snapshots, we show that the increase of angular spread reduces the mean of the detection statistics, which degrades performance, and at the same time reduces its variance, which improves performance. Within a certain range of DOF, detection performance improves

Manuscript received July 18, 2002; revised August 12, 2003. This work was supported by the Office of Naval Research under Grant N00014-01-1-0075. The associate editor coordinating the review of this manuscript and approving it for publication was Dr. Alexi Gorokhov.

The authors are with the University of California, Santa Cruz, CA 95060 USA (e-mail: yjin@cse.ucsc.edu; friedlan@cse.ucsc.edu).

Digital Object Identifier 10.1109/TSP.2004.827196

as the angular spread increases, up to a point, and then decreases slowly.

Next, we consider the case where various parameters, such as the signal direction, its angular spread, its power, and the noise power, are unknown. We derive the GLR detector and evaluate its performance by computer simulation. We show that the GLR detector has a significant performance advantage compared with the conventional beamformers as the angular spread becomes large.

The rest of the paper is organized as follows. In Section II, the signal model for a distributed source is presented and the detection problem is formulated. In Section III, various detectors are discussed, and the detection statistics are derived. The performance analysis is presented in Section IV. Finally, the computer simulation results that serve to illustrate the behavior of the detectors are presented in Section V.

Notation: Vectors (matrices) are denoted by boldface lower (upper) case letters; all vectors are column vectors; superscripts $(\cdot)^H$ denote the complex conjugate transpose; \mathbf{I}_r denotes the $r \times r$ identity matrix; $E\{\cdot\}$ denotes the statistical expectation; $|\cdot|$ denotes the matrix determinant; $\|\cdot\|$ denotes the vector (matrices) Frobenius norm; $\text{Tr}[\cdot]$ denotes the trace of a matrix.

II. PROBLEM STATEMENT

A. Signal Model

We assume that we have an array with P sensors with an array response vector $\mathbf{a}(\phi)$, where ϕ denotes azimuth. The array and all the sources are assumed to be in the same plane. We are also assuming a narrowband model for all the signals, and all the signals are defined in baseband. The signal received by the array from a single source is modeled as

$$\mathbf{x}_t = \mathbf{s}_t + \mathbf{n}_t, \quad t = 1, \dots, T \quad (1)$$

where $\mathbf{x}_t = [x_{t1}, \dots, x_{tP}]$ is the array output at sample time t . \mathbf{s}_t is the signal received at the array elements, assumed to be complex Gaussian with zero mean and covariance $E_s \mathbf{R}_s$, where E_s is the total signal power. \mathbf{R}_s will be defined in (3). \mathbf{n}_t is complex Gaussian noise with zero mean and covariance \mathbf{R}_n . The signal and noise are assumed to be uncorrelated from sample to sample. The correlation matrix of the observation vector \mathbf{x}_t is given by

$$\mathbf{R}_1 = E \{ \mathbf{x}_t \mathbf{x}_t^H \} = E_s \mathbf{R}_s(\phi, \beta) + \mathbf{R}_n \quad (2)$$

where the signal covariance matrix is given by

$$\mathbf{R}_s(\phi, \beta) = \int_{-\pi}^{\pi} P(\theta; \phi, \beta) \mathbf{a}(\theta) \mathbf{a}(\theta)^H d\theta \quad (3)$$

where ϕ is the source azimuth angle, and β is the source angular spread with $0 \leq \beta \leq 2\pi$. $\mathbf{a}(\theta)$ is the array manifold at angle θ . $\mathbf{R}_s(\phi, \beta)$ is normalized so that $\text{Tr}[\mathbf{R}_s(\phi, \beta)] = P$. $P(\theta; \phi, \beta)$ is the spatial energy distribution of the source at azimuth ϕ . More specifically, we may assume that $P(\theta; \phi, \beta) = P(\theta - \phi, \beta)$ with $\int_{-\pi}^{\pi} P(\theta; \phi, \beta) d\theta = 1$. The shape of the energy distribution function depends on the angular spread parameter β . When

$\beta = 0^\circ$, $P(\theta; \phi, \beta)$ is a unit pulse. As β increases, the energy distribution function becomes wider. For simplicity, we consider in the following an uniformly distributed source model, i.e.,

$$P(\theta; \phi, \beta) = \begin{cases} \frac{1}{\beta}, & \theta \in \left(\phi - \frac{\beta}{2}, \phi + \frac{\beta}{2}\right) \\ 0, & \text{otherwise.} \end{cases} \quad (4)$$

One can also consider a Gaussian type distribution such that

$$P(\theta; \phi, \beta) = \begin{cases} \frac{1}{\sqrt{2\pi\beta^2}} e^{-((\theta-\phi)^2/2\beta^2)}, & \theta \in \left(\phi - \frac{\beta}{2}, \phi + \frac{\beta}{2}\right) \\ 0, & \text{otherwise.} \end{cases} \quad (5)$$

B. Signal Subspace

By performing an eigen-decomposition of matrix $\mathbf{R}_s(\phi, \beta)$, we get

$$\mathbf{R}_s(\phi, \beta) = \mathbf{U} \mathbf{\Lambda} \mathbf{U}^H = (\mathbf{U}_r \quad \mathbf{U}_n) \begin{pmatrix} \Lambda_r & 0 \\ 0 & \Lambda_n \end{pmatrix} \begin{pmatrix} \mathbf{U}_r^H \\ \mathbf{U}_n^H \end{pmatrix} \quad (6)$$

where

$$\mathbf{U} = (\mathbf{U}_r \quad \mathbf{U}_n), \quad \mathbf{\Lambda} = \text{diag}(\Lambda_r, \Lambda_n) \\ \Lambda_r = \text{diag}(\lambda_1, \dots, \lambda_r). \quad (7)$$

Here, Λ_r consists of the $1 \leq r \leq P$ largest eigenvalues of $\mathbf{R}_s(\phi, \beta)$ in descending order, and $\mathbf{U}_r = (\mathbf{u}_1 \cdots \mathbf{u}_r)$ contains the corresponding orthonormal eigenvectors. If $\mathbf{R}_s(\phi, \beta)$ is a low-rank matrix with rank r , then $\mathbf{R}_s(\phi, \beta) = \mathbf{U}_r \Sigma_r \mathbf{U}_r^H$. More generally, we will assume that $\mathbf{R}_s(\phi, \beta)$ can be approximated by a rank r matrix. The number of dominant eigenvalues may be defined as the minimum number of eigenvalues whose sum exceeded τP , where $0 \leq \tau \leq 1$ is close to unity (e.g., $\tau = 0.95$). Thus

$$\mathbf{R}_s(\phi, \beta) \approx \mathbf{U}_r \Sigma_r \mathbf{U}_r^H. \quad (8)$$

The range space of \mathbf{U}_r is called the *signal subspace*, and its orthogonal complement, called the *noise subspace*, is spanned by \mathbf{U}_n . The effective rank of subspace is the number of dominant eigenvalues. The case where $\beta = 0^\circ$ corresponds to a point source where the rank $r = 1$, and signal covariance becomes $\mathbf{R}_s(\phi, 0) = \mathbf{a}(\phi) \mathbf{a}(\phi)^H$.

We notice that the effective rank of the subspace is approximately equal to the normalized angular spread by its beamwidth for a uniform spatial distribution. Fig. 1 depicts the effective rank as the angular spread changes for different size of the linear array for uniform and Gaussian-type distribution functions, respectively. For the uniform distribution, there exists a quite good match between the effective rank and the normalized angular spread, although this match degrades a bit for the Gaussian-type distribution functions. Furthermore, it is interesting to look at the profile of the eigenvalues for the uniform distribution function. As is shown in Fig. 2, the dominant principal eigenvalues concentrate within a small range. This observation suggests that we could assume that the dominant eigenvalues are approximately equal for a uniform distribution function under some circumstances.

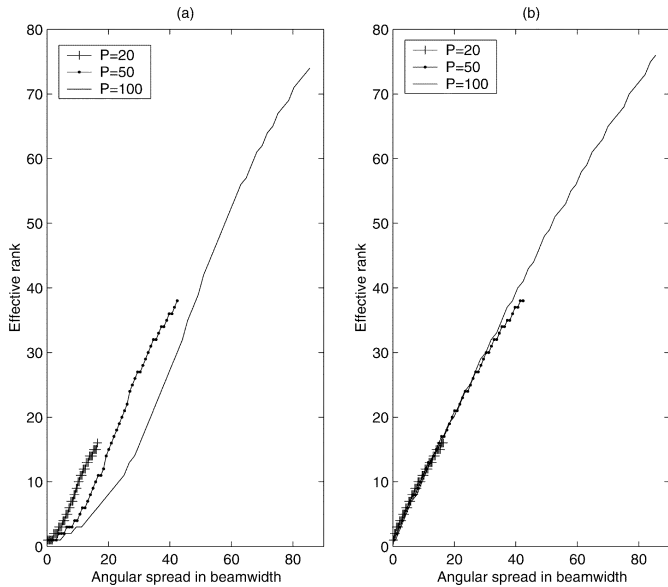


Fig. 1. Effective rank plot versus normalized angular spread in beamwidth for different spatial distribution functions. The threshold is set to 0.95. (a) Gaussian distribution. (b) Uniform distribution.

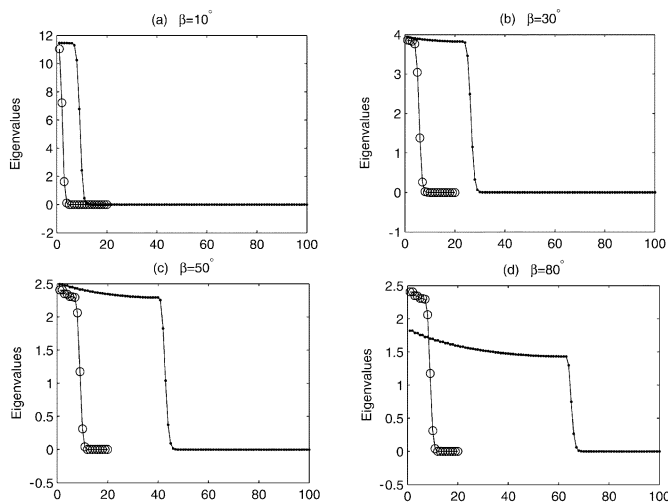


Fig. 2. Eigenvalues of the signal covariance matrix with a uniform spatial distribution for different angular spread. The dotted line depicts the eigenvalue plots of a linear array with $P = 100$ sensors, and the circled line is for a linear array with $P = 20$ sensors.

C. Detection Problem

The problem considered in this paper is of detecting a random Gaussian signal in the presence of noise and interference. The detection problem is to decide between the null hypothesis

$$H_0: \mathbf{x}_t = \mathbf{n}_t, \quad t = 1, \dots, T \quad (9)$$

and the alternative hypothesis

$$H_1: \mathbf{x}_t = \mathbf{s}_t + \mathbf{n}_t, \quad t = 1, \dots, T. \quad (10)$$

The covariance matrix of the array output under H_0 and H_1 is $\mathbf{R}_0 = \mathbf{R}_n$, and \mathbf{R}_1 defined in (2), respectively. Let us assume for the moment that the interference has characteristics similar to that of the noise and can therefore be absorbed into the noise

TABLE I
GLR DETECTORS AND BEAMFORMER DETECTORS

GLR detectors		Beamformer detectors	
detector type	unknowns	detector type	unknowns
Type I	None		
Type II	(ϕ, β)	Type IV	(ϕ)
Type III	$(\phi, \beta, E_s, \sigma^2)$	Type V	(ϕ, E_s, σ^2)

vector \mathbf{n}_t . Without loss of generality, we assume that the background noise is spatially white or $\mathbf{R}_n = \sigma^2 \mathbf{I}$, where σ^2 is the noise variance. Here, we assume that the noise level under null and alternative hypotheses does not differ. In the case where noise is spatially colored, or $\mathbf{R}_n = \sigma^2 \mathbf{R}_{nn}$, where \mathbf{R}_{nn} is a known positive definite Hermitian matrix, the detection is preceded by a whitening filter $\mathbf{R}_{nn}^{-1/2}$. We will still have binary hypotheses with \mathbf{x}_t being a whitened data vector. Consequently, we assume that the noise vectors $\{\mathbf{n}_1, \dots, \mathbf{n}_T\}$ are independent and identically distributed. The case of unknown structured interference will be presented elsewhere.

By grouping all the T snapshots of observation vectors into an observation matrix $\mathbf{X} = [\mathbf{x}_1 \cdots \mathbf{x}_T]$, we have $\mathbf{X} = \mathbf{S} + \mathbf{N}$, where the signal matrix $\mathbf{S} = [\mathbf{s}_1 \cdots \mathbf{s}_T]$ and noise matrix $\mathbf{N} = [\mathbf{n}_1 \cdots \mathbf{n}_T]$. The detection statistics depend on a set of parameters

$$p = (E_s, \phi, \beta, \sigma^2). \quad (11)$$

When all the parameters are known, this is a standard detection problem whose optimal solution is the likelihood ratio detector [22]. When the parameters are unknown, we will use the GLR approach [13], involving the replacement of unknown parameters by their maximum likelihood estimates under each hypothesis. There are several detectors that can be constructed depending on which parameters are known or unknown. We will not consider in exhaustive detail all possible combinations. Instead, we consider the GLR detectors that are the counterparts of conventional beamformers with the same set of unknown parameters so that a fair comparison between the GLR and the corresponding beamformer detectors can be made.

The detection problems to be considered in this paper are listed in Table I. The Type I detector assumes that all the parameters are known and is used as a reference. Types II and IV and Types III and V are compared when (ϕ, β) and $(E_s, \sigma^2, \phi, \beta)$ are unknown, respectively. The beamformer detectors (Types IV and V) are designed under the assumption of point sources (zero angular spread).

III. DETECTORS

We assume that the received signals under the null and alternative hypothesis are complex Gaussian with zero mean and covariance \mathbf{R}_0 and \mathbf{R}_1 , respectively, and that the probability density functions (PDFs) for the T observations are given by [3]

$$f(\mathbf{X}; H_0) = [\pi^P |\mathbf{R}_0|]^{-T} \exp \{-T \text{Tr}[\mathbf{R}_0^{-1} \mathbf{Q}]\} \quad (12)$$

$$f(\mathbf{X}; H_1) = [\pi^P |\mathbf{R}_1|]^{-T} \exp \{-T \text{Tr}[\mathbf{R}_1^{-1} \mathbf{Q}]\} \quad (13)$$

where $\mathbf{Q} = (1/T) \sum_{t=1}^T \mathbf{x}_t \mathbf{x}_t^H = (1/T) \mathbf{X} \mathbf{X}^H$ is the sample covariance matrix. We emphasize that we do not impose the

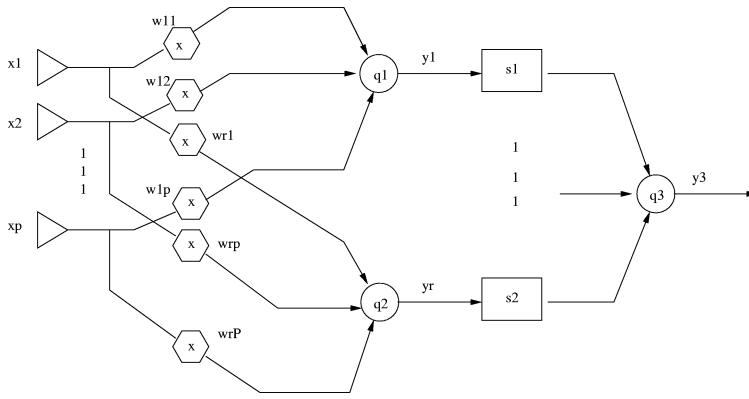


Fig. 3. Subspace beamformer configuration.

constraint that $T \geq P$. In other words, the detection can be carried out based on a single measurement ($T = 1$) or multiple measurements ($T > 1$). In an underwater acoustic scenario, large aperture arrays are often used to obtain narrow beams. The number of sensors can be in the hundreds. Therefore, detecting acoustic sources based on a few data snapshots becomes a typical problem, in which case, the sample covariance matrix \mathbf{Q} is not full rank (see, e.g., [6]). Based on the Neyman–Person theorem, when all the parameters are known, the optimal detector is the logarithm of the ratio $f(\mathbf{X}; H_1)/f(\mathbf{X}; H_0)$ of the likelihood functions. This log-likelihood ratio takes the form

$$L(\mathbf{x}) = \text{Tr}[\mathbf{X}^H (\mathbf{R}_0^{-1} - \mathbf{R}_1^{-1}) \mathbf{X}] + T \ln \frac{|\mathbf{R}_0|}{|\mathbf{R}_1|}. \quad (14)$$

Next, we consider the case where some parameters are unknown. The unknown parameters under H_0 and H_1 are denoted by p_0 and p_1 , respectively. In this case, the detection statistic is given by the GLR [13]

$$l(\mathbf{X}, \hat{p}_0, \hat{p}_1) = \frac{\max_{p_1} f(\mathbf{X}, H_1)}{\max_{p_0} f(\mathbf{X}, H_0)} \quad (15)$$

or its logarithm

$$L(\mathbf{X}, \hat{p}_0, \hat{p}_1) = \text{Tr}[\mathbf{X}^H (\mathbf{R}_0^{-1}(\hat{p}_0) - \mathbf{R}_1^{-1}(\hat{p}_1)) \mathbf{X}] + T \ln \frac{|\mathbf{R}_0(\hat{p}_0)|}{|\mathbf{R}_1(\hat{p}_1)|} \quad (16)$$

where \hat{p}_0 and \hat{p}_1 are the parameter values that maximize the likelihood function under H_0 and H_1 , respectively. In Sections III–A–C, we consider in more detail the structures of the different detectors introduced earlier. We start with the Type I detector as the optimum detector. The GLR detectors and the beamformer detectors will be discussed afterwards.

A. Subspace Beamformer—Type I

Ignoring the constant term $T \ln(|\mathbf{R}_0|/|\mathbf{R}_1|)$, we can write (14) as follows:

$$L(\mathbf{X}, p) = \text{Tr}[\mathbf{X}^H \mathbf{W} \mathbf{W}^H \mathbf{X}] \quad (17)$$

where

$$\mathbf{W} \mathbf{W}^H = \mathbf{R}_0^{-1}(p) - \mathbf{R}_1^{-1}(p) \quad (18)$$

where p is defined in (11). The above decomposition of $\mathbf{W} \mathbf{W}^H$ is possible because $\mathbf{R}_0^{-1} - \mathbf{R}_1^{-1}$ is a non-negative definite matrix. In general, \mathbf{W} is a $P \times r$ matrix, where $1 \leq r \leq P$. The rank of \mathbf{W} depends on the rank of the signal covariance matrix \mathbf{R}_s . Utilizing (2) and (8), we obtain

$$\mathbf{R}_1 \approx E_s \mathbf{U}_r \Sigma_r \mathbf{U}_r^H + \mathbf{R}_0. \quad (19)$$

Employing the matrix inversion lemma, we obtain

$$\mathbf{R}_1^{-1} \approx \mathbf{R}_0^{-1} - \mathbf{R}_0^{-1} \mathbf{U}_r (E_s \Sigma_r + \mathbf{U}_r^H \mathbf{R}_0^{-1} \mathbf{U}_r)^{-1} \mathbf{U}_r^H \mathbf{R}_0^{-1}. \quad (20)$$

Hence, we can rewrite (18) as follows:

$$\mathbf{W} \mathbf{W}^H \approx \mathbf{R}_0^{-1} \mathbf{U}_r (E_s \Sigma_r + \mathbf{U}_r^H \mathbf{R}_0^{-1} \mathbf{U}_r)^{-1} \mathbf{U}_r^H \mathbf{R}_0^{-1} \quad (21)$$

and then, the subspace matrix is a $P \times r$ matrix

$$\mathbf{W} \approx \mathbf{R}_0^{-1} \mathbf{U} (E_s \Sigma + \mathbf{U}^H \mathbf{R}_0^{-1} \mathbf{U})^{-1/2} = [\mathbf{w}_1, \dots, \mathbf{w}_r]. \quad (22)$$

If the signal subspace is indeed low rank with rank r , the approximation sign is replaced by an equality sign. This leads to an interpretation of the LR detector as a bank of beamformers. We emphasize that in general, this subspace beamformer is an approximation to the true LR detector. In our case, the noise covariance matrix $\mathbf{R}_n = \sigma^2 \mathbf{I}$, which leads to a simpler form

$$\mathbf{W} \approx \frac{1}{\sigma^2} \mathbf{U}_r \left(\frac{1}{\sigma^2} \mathbf{U}_r^H \mathbf{U}_r + E_s \Sigma_r \right)^{-1/2}. \quad (23)$$

We denote \mathbf{Y} as an output matrix of the beamformers, or

$$\mathbf{Y} = \mathbf{W}^H \mathbf{X} = [\mathbf{y}_1 \dots \mathbf{y}_T] \quad (24)$$

where $\mathbf{y}_t = \mathbf{W}^H \mathbf{x}_t$. We will refer to this as a “subspace beamformer” (see Fig. 3) to distinguish it from the conventional beamformer, where \mathbf{w} is a $P \times 1$ vector. The detection statistic is given by

$$L(\mathbf{X}, p) = \text{Tr}[\mathbf{Y} \mathbf{Y}^H] = \sum_{t=1}^T \|\mathbf{y}_t\|^2 \quad (25)$$

where $\|\mathbf{y}_t\|^2$ is the sum of squared magnitudes of the subspace beamformer outputs. A plot of the normalized array directional pattern in decibels for a 20-element linear array is given in Fig. 4. The array pattern of the subspace beamformer shows a

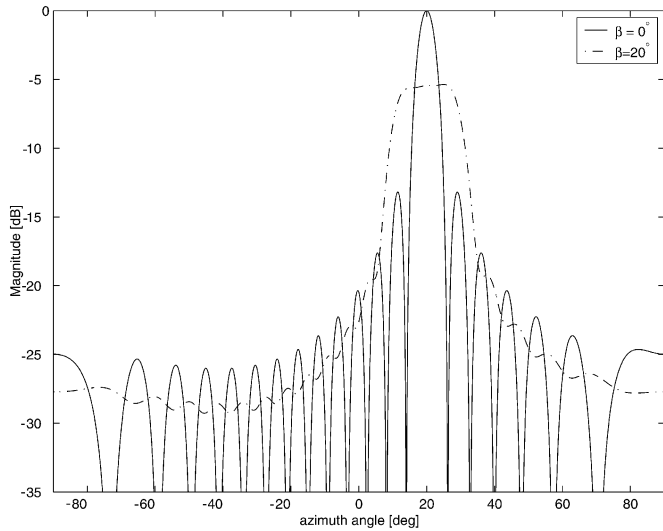


Fig. 4. Subspace beamformer array pattern for a 20-element, half wavelength spaced linear array. The solid line with an angular spread $\beta = 0^\circ$ corresponds to the conventional beamformer. The dashed line with $\beta = 20^\circ$ has dropoff of 6 dB compared with conventional beamformer. The dropoff is equal to the effective rank $r = 4$ of the signal subspace in decibels. The source direction is 20° relative to the broadside of the array.

dropoff of 6 dB, which reflects an SNRG reduction. A more detailed analysis is provided in Section IV-A. The detection statistic $L(\mathbf{X})$ is distributed as a weighted Chi-squared random variable (see Section IV-B for details).

B. GLR Detectors

Type II: In this case, the unknown parameter $p = (\phi, \beta)$ needs to be estimated. Note that the likelihood function under H_0 is independent of p , and thus, it needs to be estimated only under H_1 . The detection statistics are constructed as follows by maximizing argument p :

$$L(\mathbf{X}, \hat{p}_1) = \text{Tr}[\mathbf{X}^H (\mathbf{R}_0^{-1} - \mathbf{R}_1^{-1}(\hat{p}_1)) \mathbf{X}] + T \ln \frac{|\mathbf{R}_0|}{|\mathbf{R}_1(\hat{p}_1)|} \quad (26)$$

where $\hat{p}_1 = \arg \max_{\phi \in (-\pi/2, \pi/2), \beta \in (0, \beta_0)} L(\mathbf{X}, p_1)$. The estimation is done by a numerical maximization over the range $-\pi \leq \phi \leq \pi$ (or $-\pi/2 \leq \phi \leq \pi/2$ for a linear array), and $0 \leq \beta \leq \beta_0$, where β_0 is a predetermined angular spread range. The maximization is carried out by the following steps.

- *Step 1.* We divide a two-dimensional search range (β, ϕ) into small grids. The size of the grid $(\delta\beta, \delta\phi)$ is a fraction of an array beamwidth. We choose $\delta\beta = \alpha_1 BW$ and $\delta\phi = \alpha_2 BW$, where $0 < \alpha_1, \alpha_2 < 1$. We find that $\alpha_1, \alpha_2 = 0.5$ produce quite reliable results.
- *Step 2.* For every pair of (β_i, ϕ_i) , $\mathbf{R}_s(\beta_i, \phi_i)$ is constructed based on (3).
- *Step 3.* The detection statistic $L(\mathbf{X}; (\beta_i, \phi_i))$ is evaluated.
- *Step 4.* This process is repeated, and the largest value of $L(\mathbf{X}; (\beta_i, \phi_i))$ is selected.

Type III: In this case, all the parameters are unknown. The ML method requires a nonlinear optimization. The detector searches the global maximum of the likelihood function over

the unknown parameter sets. The maximization can be carried out as follows:

$$\begin{aligned} l(\mathbf{X}, \hat{\rho}, \hat{\sigma}_1^2, \hat{\sigma}_0^2, \hat{p}_1) &= \max_{p_1} l(\mathbf{X}, \hat{\rho}, \hat{\sigma}_1^2, \hat{\sigma}_0^2, p_1) \\ &= \max_{p_1} \max_{\rho \in (0, \rho_0)} l(\mathbf{X}, \rho, \hat{\sigma}_1^2, \hat{\sigma}_0^2, p_1) \end{aligned} \quad (27)$$

where the SNR $\rho = E_s/\sigma^2$. We first maximize likelihood function over (ρ, σ^2) , assuming that $p_1 = (\beta, \phi)$ are known. We then maximize the result over (β, ϕ) . We find it convenient to reparameterize (E_s, σ^2) as (ρ, σ^2) . This reparameterization does not alter the maximum of the likelihood function in that there is a one-to-one mapping between the two parameter sets.

The derivation of the maximum likelihood estimators of (ρ, σ^2) is provided in Appendix for a fixed p_1 . The GLR takes the form

$$l(\mathbf{X}, \hat{\rho}, \hat{\sigma}_1^2, \hat{\sigma}_0^2, p_1) = \left(\frac{\text{Tr}[\mathbf{Q}]}{\text{Tr}[(\hat{\rho}\mathbf{R}_s(p_1) + \mathbf{I})^{-1}\mathbf{Q}]} \right)^{PT} \times \frac{1}{|\hat{\rho}\mathbf{R}_s(p_1) + \mathbf{I}|^T}. \quad (28)$$

Taking the logarithm of the equation above leads to the following detection statistics:

$$L(\mathbf{X}, \hat{\rho}, \hat{\sigma}_1^2, \hat{\sigma}_0^2, p_1) = PT \ln \left(\frac{\text{Tr}[\mathbf{Q}]}{\text{Tr}[(\hat{\rho}\mathbf{R}_s(\hat{p}_1) + \mathbf{I})^{-1}\mathbf{Q}]} \right) - T \ln |\hat{\rho}\mathbf{R}_s(\hat{p}_1) + \mathbf{I}| \quad (29)$$

where $\hat{p}_1 = \arg \max_{-\pi/2 \leq \phi \leq \pi/2, 0 \leq \beta \leq \beta_0} L(\mathbf{X}, \hat{\rho}, \hat{\sigma}_0^2, \hat{\sigma}_1^2, p_1)$. In summary, the maximization is carried out as follows.

- *Step 1.* Follow Steps 1 and 2 for the type II detector.
- *Step 2.* For each pair of (β_i, ϕ_i) , a one-dimensional search over ρ is carried out to select the maximal value of $L(\mathbf{X}, (\beta_i, \phi_i), \rho)$. The search can be implemented through a binary search or an exhaustive search. ρ_0 is a predetermined search range.
- *Step 3.* This process is repeated for all the values of (β_i, ϕ_i) , and the largest value of $L(\mathbf{X}, (\beta_i, \phi_i), \rho)$ is selected.

C. Beamformers

Type IV: This beamformer searches for the maximum energy by sweeping over all possible directions. This is the optimal solution (maximum likelihood) for point sources. However, if the source is distributed, only a fraction of the energy is captured by the beamformer. Consequently, a degradation in performance will occur. For a linear array, the beamformer searches over $-\pi/2 \leq \phi \leq \pi/2$. The detection statistic is

$$L(\mathbf{X}) = \|\mathbf{w}^H(\hat{\phi})\mathbf{X}\|^2 \quad (30)$$

where $\hat{\phi} = \arg \max_{-\pi/2 \leq \phi \leq \pi/2} \|\mathbf{w}^H(\phi)\mathbf{X}\|^2$, and $\mathbf{a}(\phi)$ is the steering vector pointing to direction ϕ . The implementation of this beamformer detector is quite straightforward. The beamformer detector \mathbf{w} is a normalized steering vector. The maximal value of detection statistic is chosen by sweeping the beamformer from $-\pi/2$ to $\pi/2$.

Type V: This is a constant false alarm rate (CFAR) beamformer similar to the matched subspace detector in [22]. This beamformer searches the maximum energy output over the range $-\pi/2 \leq \phi \leq \pi/2$. The signal energy is divided by an estimate of the noise variance that is calculated by projecting the array output on the subspace orthogonal to the rank 1 steering vector. To exclude the signal power that “leaks” through the beams adjacent to the main beam, we estimate the noise power from beams that are further away from the main beam. For example, we can choose to exclude the β_0/BW beams adjacent to the main beam, where β_0 is a predetermined angular spread range. This seemingly *ad hoc* approach is a modified maximum likelihood estimate of the noise variance. It is well known that the estimate of noise variance is given by [16]

$$\hat{\sigma}^2 = \frac{\|\mathbf{P}_{\mathbf{A}}^\perp \mathbf{x}\|^2}{(P - r_{\mathbf{A}})} \quad (31)$$

where \mathbf{A} is the signal subspace, and $r_{\mathbf{A}}$ is the rank of the signal subspace. The accuracy of the noise estimate will degrade when a smaller subspace is used due to the leakage of the signal power onto the noise subspace. Hence, we construct a subspace $\mathbf{B} \supseteq \mathbf{A}$ so that the signal power is excluded from the estimation. In other words, a subspace $\mathbf{B}(\phi, \beta_0) = [\mathbf{a}(\phi - \beta_0/2), \dots, \mathbf{a}(\phi + \beta_0/2)]$ is generated. The power that is projected onto the null space of $\mathbf{B}(\phi, \beta_0)$ is considered to be the noise power, i.e.,

$$\hat{\sigma}^2(\beta_0, \phi) = \frac{\text{Tr}[\mathbf{P}_{\mathbf{B}(\beta_0, \phi)}^\perp \mathbf{Q}]}{(P - r_{\mathbf{B}})} \quad (32)$$

where $\mathbf{P}_{\mathbf{a}(\phi)}$ is the projection matrix on $\mathbf{a}(\phi)$, and $\mathbf{P}_{\mathbf{B}(\beta_0, \phi)}^\perp = \mathbf{I} - \mathbf{P}_{\mathbf{B}(\beta_0, \phi)}$. $r_{\mathbf{B}}$ is the rank of \mathbf{B} . The detection statistic of this CFAR detector is given as follows:

$$L(\mathbf{X}) = \max_{\phi \in (-\pi/2, \pi/2)} \frac{\text{Tr}[\mathbf{P}_{\mathbf{a}(\phi)} \mathbf{Q}]}{\hat{\sigma}^2(\beta_0, \phi)}. \quad (33)$$

The implementation of this detector involves three steps.

- *Step 1.* For every angle ϕ , we construct a projection matrix $\mathbf{P}_{\mathbf{a}(\phi)}$. A subspace $\mathbf{B}(\phi, \beta_0)$ and a null projection matrix $\mathbf{P}_{\mathbf{B}(\beta_0, \phi)}^\perp$ are constructed accordingly.
- *Step 2.* The detector output is evaluated based on (33) for every angle ϕ .
- *Step 3.* The largest value of $L(\mathbf{X}, (\beta_i, \phi_i), \rho)$ is selected.

IV. PERFORMANCE ANALYSIS OF THE TYPE I DETECTOR

In this section, we analyze the performance of the proposed type I subspace beamformer by developing analytical expressions for its SNRG and the receiver operating characteristics (ROCs).

A. SNRG versus Angular Spread

SNRG is defined as the ratio of the array output to input SNRs. For point sources, the SNRG depends on the number of sensors. For a linear array with P sensors $\text{SNRG} = P$. Next, we derive the SNRG for the subspace beamformers. The subspace beamformer output is

$$\mathbf{y}_t = \mathbf{W}^H \mathbf{x}_t = \mathbf{W}^H \mathbf{s}_t + \mathbf{W}^H \mathbf{n}_t. \quad (34)$$

Let the output SNR (SNRO) be the average signal power divided by the average noise power at the beamformer output

$$\begin{aligned} \text{SNRO} &= \frac{\text{Tr}[\mathbf{W}^H E\{\mathbf{s}_t \mathbf{s}_t^H\} \mathbf{W}]}{\text{Tr}[\mathbf{W}^H E\{\mathbf{n}_t \mathbf{n}_t^H\} \mathbf{W}]} = \frac{\text{Tr}[E_s \mathbf{W}^H \mathbf{R}_s \mathbf{W}]}{\text{Tr}[\mathbf{W}^H \mathbf{R}_n \mathbf{W}]} \\ &= \frac{E_s}{\sigma^2} \frac{\text{Tr}[\mathbf{W}^H \mathbf{R}_s \mathbf{W}]}{\text{Tr}[\mathbf{W}^H \mathbf{W}]} \end{aligned} \quad (35)$$

The input SNR is $\text{SNR} = E_s/\sigma^2$. The signal to noise ratio gain is $\text{SNRG} = \text{SNRO}/\text{SNR} = \text{Tr}[\mathbf{W}^H \mathbf{R}_s \mathbf{W}]/\text{Tr}[\mathbf{W}^H \mathbf{W}]$. We are interested in how the SNRG of the subspace beamformer varies with the signal angular spread. Note that

$$\begin{aligned} \mathbf{W} \mathbf{W}^H &= \frac{1}{\sigma^2} \mathbf{I} - (\sigma^2 \mathbf{I} + E_s \mathbf{R}_s(\beta))^{-1} \\ &\approx \mathbf{U}_r \left[\frac{1}{\sigma^2} \mathbf{I} - (\sigma^2 \mathbf{I} + E_s \Lambda_r)^{-1} \right] \mathbf{U}_r^H \\ &= \mathbf{U}_r \mathbf{D} \mathbf{U}_r^H \end{aligned} \quad (36)$$

where

$$\mathbf{D} = \text{diag}[E_s \lambda_1 / \sigma^2 (\sigma^2 + E_s \lambda_1), \dots, E_s \lambda_r / \sigma^2 (\sigma^2 + E_s \lambda_r)].$$

Λ_r is defined in (7). Hence, we have

$$\text{SNRG} \approx \frac{\text{Tr}[\mathbf{D} \Lambda_r]}{\text{Tr}[\mathbf{D}]} = \frac{\sum_{i=1}^r \frac{\lambda_i^2}{1 + \text{SNR} \lambda_i}}{\sum_{i=1}^r \frac{\lambda_i}{1 + \text{SNR} \lambda_i}}. \quad (37)$$

For simplicity, we assume that the dominant eigenvalues are *approximately* equal, i.e., $\lambda_i = P/r$, $i = 1 \dots r$. This approximation is certainly not very accurate, but it reveals some insights of the behavior of SNRG. Therefore, we obtain

$$\text{SNRG} \approx \frac{P}{r}. \quad (38)$$

This result shows that the SNRG for the subspace beamformer not only depends on the number of sensors P but on source angular spread β through subspace rank r as well. It is a monotone decreasing function of r . The following can be concluded as two special cases.

- 1) For the point source case $\beta = 0^\circ$ or $\mathbf{R}_s = \mathbf{a} \mathbf{a}^H$, we get $\text{SNRG} = P$.
- 2) For the case $\beta = 2\pi$ or $\mathbf{R}_s = \mathbf{I}$, we get unit gain $\text{SNRG} = 1$.

B. Receiver Operating Characteristics

In this section we derive an analytical expression of PDFs under two hypotheses. In what follows, we write χ_{M}^2 to denote the central Chi-squared distribution with M degrees of freedom and $p_M(z)$ to be the pdf of a central Chi-squared distribution with M degrees of freedom. The log-likelihood ratio under hypothesis H_i , $i = 0, 1$ is

$$\begin{aligned} L(\mathbf{X}, H_i) &= \mathbf{X}^H \mathbf{W} \mathbf{W}^H \mathbf{X} \\ &= \sum_{t=1}^T \mathbf{x}_{t, H_i}^H (\mathbf{R}_0^{-1} - \mathbf{R}_1^{-1}) \mathbf{x}_{t, H_i} \\ &= \sum_{t=1}^T \sum_{j=1}^r \lambda_j |\mathbf{u}_j^H \mathbf{x}_{t, H_i}|^2 \end{aligned} \quad (39)$$

is a quadratic form in complex Gaussian random variables, where $\{\lambda_j\}$ are nonzero eigenvalues of matrix $\mathbf{W}\mathbf{W}^H$, $\{\mathbf{u}_j\}$ are the associated eigenvectors. Equation (39) can be further written as

$$L(\mathbf{X}, H_i) = \sum_{t=1}^T \sum_{j=1}^r \gamma_{ji} |z_{jit}|^2, \quad i = 0, 1 \quad (40)$$

where z_{jit} are independent zero mean unit variance complex Gaussian random variables, and $\{\gamma_{ji}, j = 1, \dots, r\}$ are the r real nonzero weights. More precisely

$$\gamma_{j0} = \frac{E_s \lambda_j}{E_s \lambda_j + \sigma^2}, \quad \gamma_{j1} = \frac{E_s \lambda_j}{\sigma^2}, \quad j = 1, \dots, r \quad (41)$$

where λ_j are the eigenvalues of \mathbf{R}_s . As a straightforward extension of the results in [5] from real numbers to complex numbers, the quadratic form $L(\mathbf{X}, H_i)$ is distributed approximately as a scaled Chi-squared random variable, or $L(\mathbf{X}, H_i) \sim \tau_i \chi_{M_i}^2$, where the scaling factor τ_i and the degrees of freedom M_i are given by

$$\tau_i = \frac{\sum \gamma_{ji}^2}{\sum \gamma_{ji}}, \quad M_i = 2T \frac{(\sum \gamma_{ji})^2}{\sum \gamma_{ji}^2}. \quad (42)$$

Plugging (41) into (42), we obtain

$$\tau_1 = \frac{\rho}{P} \sum_{j=1}^r \lambda_j^2, \quad \tau_0 = \frac{\sum_{j=1}^r \left(\frac{\rho \lambda_j}{\rho \lambda_j + 1} \right)^2}{\sum_{j=1}^r \frac{\rho \lambda_j}{\rho \lambda_j + 1}} \quad (43)$$

$$M_1 = \frac{2TP^2}{\sum_{j=1}^r \lambda_j^2}, \quad M_0 = 2T \frac{\left(\sum_{j=1}^r \frac{\rho \lambda_j}{\rho \lambda_j + 1} \right)^2}{\sum_{j=1}^r \left(\frac{\rho \lambda_j}{\rho \lambda_j + 1} \right)^2}. \quad (44)$$

Utilizing the Jacobian transformation, we can show that the pdf of detection statistics $L(\mathbf{X}, H_i)$ is $(1/|\tau_i|)p_{M_i}(z/\tau_i)$. Note that the absolute sign can be ignored because τ_i is a positive number. This leads to an approximation of the probability of false alarm (P_{FA}) and probability of detection (P_D)

$$P_{FA} \approx \int_{\eta}^{\infty} p_{M_0}(z) dz, \quad P_D \approx \int_{(\tau_0/\tau_1)\eta}^{\infty} p_{M_1}(z) dz \quad (45)$$

where the distribution function is given by

$$p_{M_i}(u) = \frac{1}{2^{M_i/2} \Gamma(\frac{M_i}{2})} u^{(1/2)M_i - 1} e^{-(1/2)u}. \quad (46)$$

Let $\psi_M(\eta) = \int_0^\eta p_M(z) dz$ denote cumulative distribution function of a Chi-squared random variable with M degrees of freedom, and let $\psi_M^{-1}(\cdot)$ be the inverse function of $\psi_M(\cdot)$. Therefore, the false alarm probability (P_{FA}) and detection probability (P_D) of quadratic form $L(\mathbf{X}, H_i)$ can be written as

$$P_D \approx 1 - \psi_{M_1} \left(\frac{\tau_0}{\tau_1} \eta \right), \quad P_{FA} \approx 1 - \psi_{M_0}(\eta). \quad (47)$$

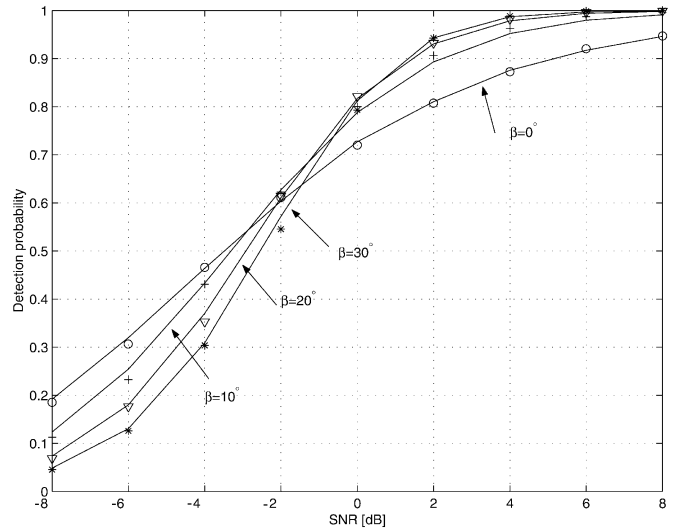


Fig. 5. Probability of detection versus SNR for Type I detector for $\beta = 0^\circ, 10^\circ, 20^\circ, 30^\circ$. The number of sensors $P = 20$. The false alarm rate $P_{FA} = 10^{-3}$. The number of measurements $T = 1$. The lines depict the analytical results, whereas the markers show Monte Carlo simulation trial results.

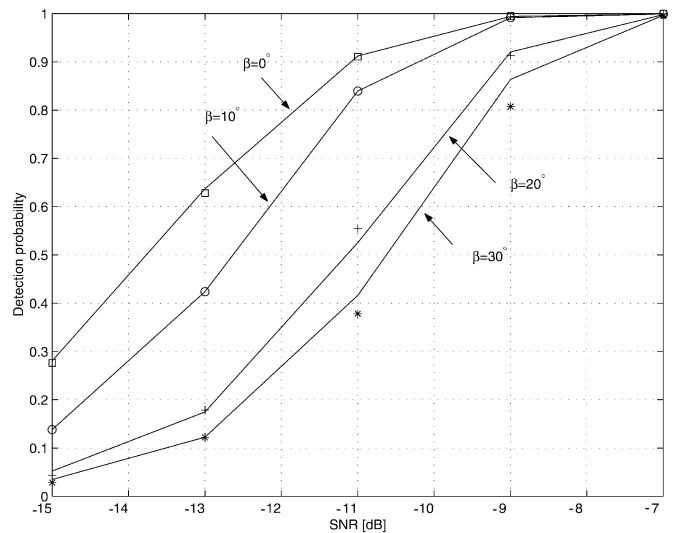


Fig. 6. Probability of detection versus SNR for Type I detector for $\beta = 0^\circ, 10^\circ, 20^\circ, 30^\circ$. The number of sensors $P = 20$. The false alarm rate $P_{FA} = 10^{-3}$. The number of measurements $T = 20$. The lines depict the analytical results, whereas the markers show Monte Carlo simulation trial results.

For a fixed level of false alarm rate, we have a closed-form expression of detection probability

$$P_D \approx 1 - \psi_{M_1} \left(\frac{\tau_0}{\tau_1} \psi_{M_0}^{-1}(1 - P_{FA}) \right). \quad (48)$$

Later, the computer simulation shows that the analytical result (the lines) matches the Monte Carlo simulation result (the markers) quite well for different number of measurements, signal angular spreads, and false alarm rate (see Figs. 5–7).

The asymptotic performance of P_D as T is sufficiently large can also be obtained in that the Chi-squared distribution with M degrees of freedom tends to become a Gaussian normal distribution with mean M and variance $2M$. Hence, when M is

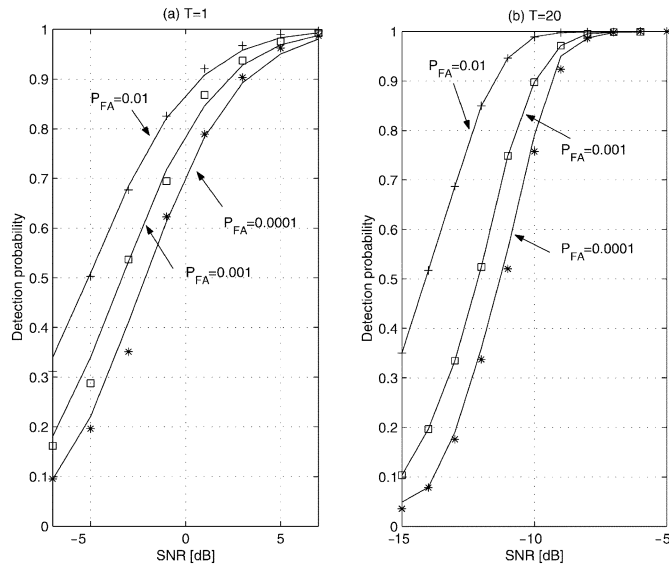


Fig. 7. Probability of detection versus SNR for Type I detector with $\beta = 10^\circ$. The number of sensors is $P = 20$. The false alarm rate is set to be $P_{FA} = 10^{-2}$, 10^{-3} , and 10^{-4} . The lines depict the analytical results, whereas the markers show Monte Carlo simulation trial results. (a) $T = 1$ measurement. (b) $T = 20$ measurements.

sufficiently large, $\psi_M(x) \rightarrow \Psi(x - M/\sqrt{2M})$, where $\Psi(x) = \int_{-\infty}^x (1/\sqrt{2\pi})e^{-1/2u^2} du$. This leads to

$$P_D \approx 1 - \Psi \left(\frac{\frac{\tau_0}{\tau_1} (M_0 + \sqrt{2M_0}\Psi^{-1}(1 - P_{FA})) - M_1}{\sqrt{2M_1}} \right). \quad (49)$$

C. Required SNR (RSNR)

The ROC describes the behavior of detection probability (P_D) as the SNR changes given a probability of false alarm (P_{FA}). To compare different detector performance, it is sometimes convenient to define a scalar performance measure, rather than use the entire ROC curve. We define the required SNR (RSNR) as the SNR needed to produce a target detection probability at a given false alarm rate.

Another quantity of interest is the output SNR ($\text{RSNR} \times \text{SNRG}$) required to achieve the same target P_D for a fixed P_{FA} . From (47), we obtain $\tau_1/\tau_0 = \psi_{M_1}^{-1}(1 - P_{FA})/\psi_{M_0}^{-1}(1 - P_D)$. Further simplification leads to

$$\rho = \frac{P}{\sum_{i=1}^r \lambda_j^2} \frac{\left(\sum_{j=1}^r \frac{\rho \lambda_j}{\rho \lambda_j + 1} \right)^2}{\sum_{j=1}^r \left(\frac{\rho \lambda_j}{\rho \lambda_j + 1} \right)^2} \frac{\psi_{M_1}^{-1}(1 - P_{FA})}{\psi_{M_0}^{-1}(1 - P_D)}. \quad (50)$$

This ρ is the RSNR. The general behavior of the quantity RSNR depends on the eigenvalues, which has certain distributions [11]. Equation (50) is quite complicated. To gain some insights of this quantity, we look at the case where all the principal eigenvalues of \mathbf{R}_s are approximately equal, i.e., $\lambda_i = \lambda = P/r$, $i = 1 \dots r$. This approximation is certainly not accurate but serves for simplicity purposes to illustrate the performance of RSNR as the degrees of freedom changes. A more accurate result may be obtained by a numerical approach. With this assumption, we have $M_0 \approx 2Tr$, $M_1 \approx 2Tr$. Let $v = 2Tr$ denote

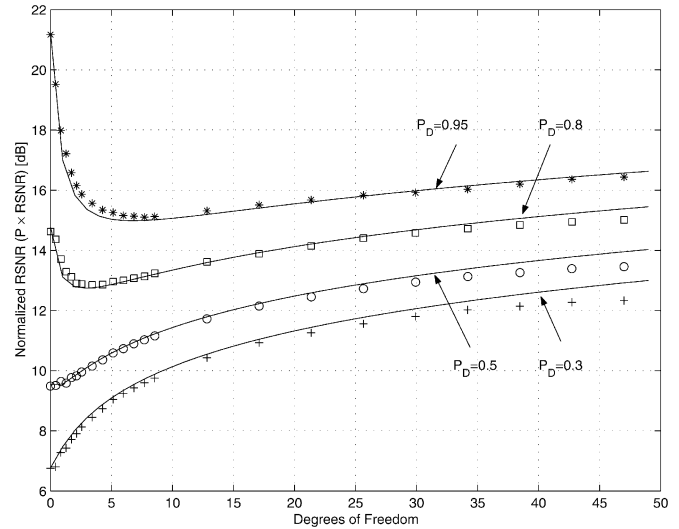


Fig. 8. Normalized RSNR versus degrees of freedom ($v \in [1, 50]$) for different target $P_D = [0.95, 0.8, 0.5, 0.3]$. The lines depict the analytical results, whereas the markers depict the Monte Carlo trial results. P_{FA} is set to be 0.001.

the degrees of freedom, and after some algebraic manipulations, we get $\text{RSNR} \approx (v/2P) (\psi_v^{-1}(1 - P_{FA})/\psi_v^{-1}(1 - P_D) - 1)$, and the quantity output SNR is given as

$$\text{RSNR} \times \text{SNRG} \approx T \left(\frac{\psi_v^{-1}(1 - P_{FA})}{\psi_v^{-1}(1 - P_D)} - 1 \right). \quad (51)$$

The quantity RSNR, which is a function of (v, P_D, P_{FA}), can be easily evaluated by numerical method. For a fixed P_{FA} , Fig. 8 depicts the RSNR for different values of degrees of freedom v and P_D . To eliminate the effect of size of the linear array, we multiply the RSNR by array size P . It is easy to see that the normalized RSNR (e.g., $P \times \text{RSNR}$) is a quantity that depends on the degrees of freedom (v), P_D and P_{FA} . This observation indicates that although the increase of the angular spread causes a reduction of SNRG, it changes the distribution of the detection statistics by increasing its degrees of freedom. This figure also explains the different behavior of detection performance, as is depicted in Figs. 5 and 6. Detectors operating in a meaningful detection range require a large target P_D . In this case, the RSNR performance improves as the degrees of freedom increase to a certain point, and then, it starts dropping. Large T or large angular spread gives rise to an asymptotic performance of the RSNR. As the degrees of freedom become large, either due to a large number of measurements or large angular spread, the detection performance degrades, but the degradation is not significant.

V. NUMERICAL EXAMPLES

In this section, we present computer simulations to illustrate the analytical performance results discussed above. We consider a uniform linear array with P sensors and half a wavelength spacing. The array manifold is given by $\mathbf{a}(\phi) = [1, e^{j2\pi(d/\lambda)\sin\phi}, \dots, e^{j2\pi((P-1)d/\lambda)\sin\phi}]^T$, where λ is the wavelength of the received signals, $d = \lambda/2$ is the element spacing, and ϕ is the azimuth angle. We find that it is convenient to normalize the angular spread by the array beamwidth

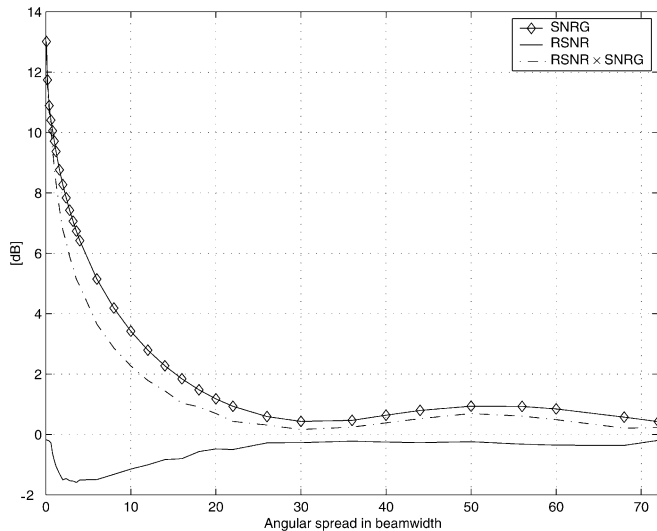


Fig. 9. SNRG and RSNR versus normalized angular spread for an array with $P = 20$ sensors. Dashed line shows the SNR gain of 13 dB at $\beta = 0^\circ$ and gain of 1 dB at $\beta = 360^\circ$. Solid line is the RSNR. The RSNR plot is computed with $P_D = 0.8$ and $P_{FA} = 10^{-3}$ based on a single measurement ($T = 1$).

(BW) [14]. We choose $P = 20$; thus, the beamwidth of this linear array is 6.03° . We assume that the source is located at 20° relative to the broadside of the array. Throughout the simulation, the probability of false alarm rate and the target detection probability are set to $P_{FA} = 10^{-3}$ and $P_D = 0.8$. We are interested in the case where there are a few snapshots available for detection; this is typically the case when the source is moving in underwater acoustic scenario so that the number of data snapshots is limited. In the simulation, we will study the cases where $T = 1$ and $T = 20$, respectively. A more detailed discussion of detection by multiple measurements is provided in [9]. The Monte Carlo simulation used 10 000 trials for each SNR.

A. ROC, RSNR, and SNRG for Type I Detector

Figs. 5–7 depict the probability of detection of a type I detector for different angular spreads β , false alarm rate P_{FA} , and number of measurements T . The figures show both the analytical results using the formulas presented earlier and the Monte Carlo trial results. We observe that there exists a very good match between the two sets of results. We notice that the behaviors of the P_D are quite different when multiple measurements are used compared with that of the single measurement detection. For single measurement (see Fig. 5), there is a crossover point of ROC curves for different angular spreads. We observe that as the angular spread increases from 0° to 30° , the detection probability performance improves up to a point, and then, it starts decreasing. However, when multiple measurements are used, the detection performance drops as the angular spread increases (see Fig. 6). This phenomenon is due to the change of the shape of the PDF whose degrees of freedom are affected by both the angular spread and the number of measurements. An alternative way of looking at this phenomenon is by studying the RSNR curves, as depicted in Fig. 8.

Fig. 9 depicts the behavior of SNRG and RSNR versus the angular spread. The SNRG plot decreases monotonically from

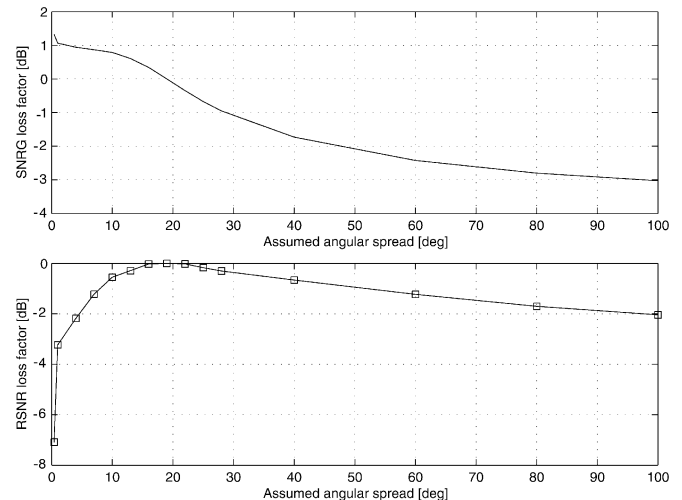


Fig. 10. SNRG and RSNR loss factor versus assumed angular spread α when there is an angular spread mismatch. The array has $P = 20$ sensors. The signal angular spread $\beta = 20^\circ$.

13 to 1 dB as the angular spread increases from $\beta = 0^\circ$ to $\beta = 360^\circ$. The output RSNR (RSNR \times SNRG dashed line) shows a performance improvement caused by the change of the PDF of the detection statistics as the angular spread increases. As the angular spread (and the effective rank of the detector subspace) increases, the PDF of the detection statistics becomes a Gaussian distribution. Once the PDF is sufficiently close to Gaussian, no more improvement occurs. The RSNR plot, which is the difference of these two plots, decreases up to a point and increases afterwards.

B. RSNR and SNRG for Detectors with an Angular Spread Mismatch

In this example, we examine the effects of angular spread mismatch on detection performance. In Fig. 10, the upper plot depicts the SNRG loss factor defined as the ratio of the SNRG for a subspace beamformer using an incorrect angular spread to that of a beamformer that uses the correct angular spread of 20° . The plot shows that as the assumed angular spread becomes larger than the correct one, the loss increases. This is due to the fact that the noise power projected on the detector subspace is proportional to the effective rank of the subspace, which increases with the assumed angular spread. The lower plot depicts RSNR loss factor as the assumed angular spread changes. The detector with the correct angular spread has the best performance. The conventional beamformer detector assumed a zero angular spread and experienced a loss of approximately 7 dB in this case.

C. Detection Performance versus Angular Spread for the GLR and the Beamformer Detectors

For a fixed false alarm rate $P_{FA} = 10^{-3}$, we study the detection probability of various detectors. The GLR detectors search over ranges of direction ϕ and angular spread β to find the maximal value of likelihood function. The search is carried out over the range $-90^\circ \leq \phi \leq 90^\circ$ and $0 \leq \beta \leq \beta_0$, where β_0 is set to be 60° . Figs. 11 and 12 depict P_D and RSNR versus angular spread for different detectors with single measurement ($T = 1$). The results show that when the angular spread is small, there is little

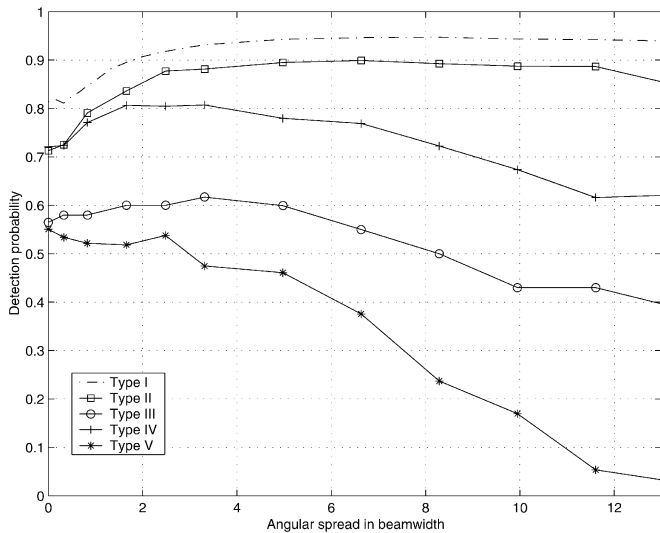


Fig. 11. Detection probability versus normalized angular spread for Type I, II, III, IV, and V detectors. The number of measurement is $T = 1$, $\text{SNR} = 2$ dB, and $P_{FA} = 10^{-3}$.

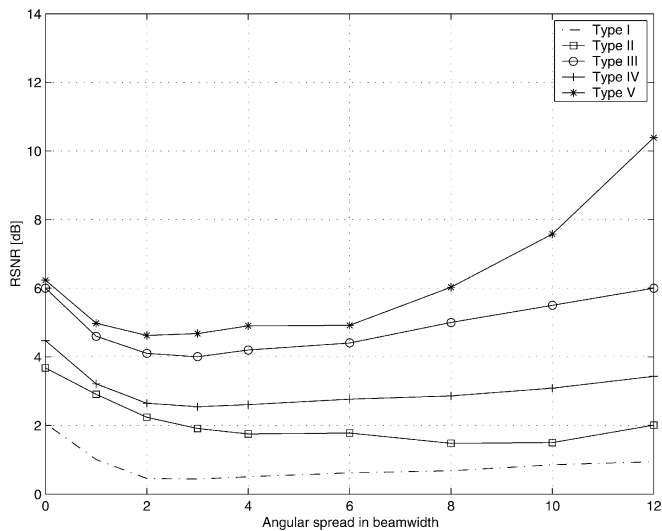


Fig. 12. RSNR versus normalized angular spread for Type I, II, III, IV, and V detectors. The number of measurement is $T = 1$. The target detection probability rate $P_D = 0.8$, and the false alarm rate $P_{FA} = 10^{-3}$.

difference between the GLR detectors and the beamformer detectors because the source appears to be a point-like source. The main beam of the beamformer detectors is able to capture all the energy coming from the source. Actually, the GLR detectors have slightly worse performance than that of the conventional beamformer detectors due to the excessive search, which results in an increase of detection threshold. As the angular spread gets larger, the performance of both the GLR detectors and the beamformer detectors degrades. However, the degradation of the beamformer detector is much more significant than that of the GLR detectors. Hence, in the case of large angular spread, the GLR detectors demonstrate a better detection probability than the comparable beamformer detectors. We also plot the type I detector as a reference in order to see how much performance dropoff that occurs for other suboptimal detectors.

Next, we study the detector performance when multiple measurements ($T = 20$) are used. In Figs. 13 and 14, we compare

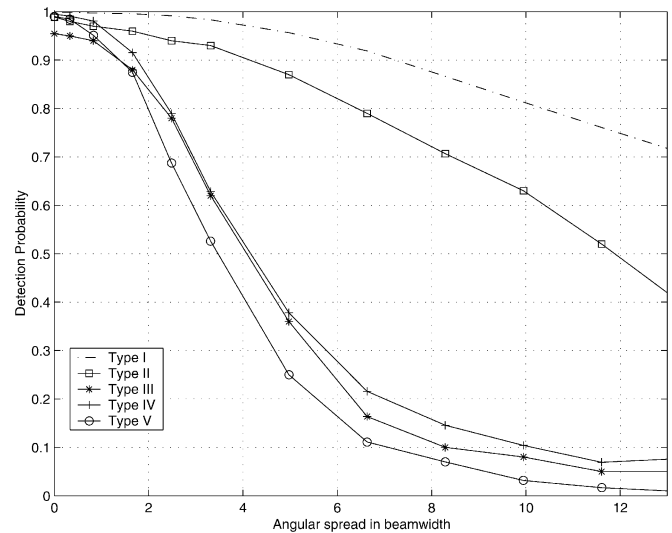


Fig. 13. Detection probability versus normalized angular spread for Type I, II, III, IV, and V detectors. The number of measurements is $T = 20$, $\text{SNR} = -8$ dB, and $P_{FA} = 10^{-3}$.

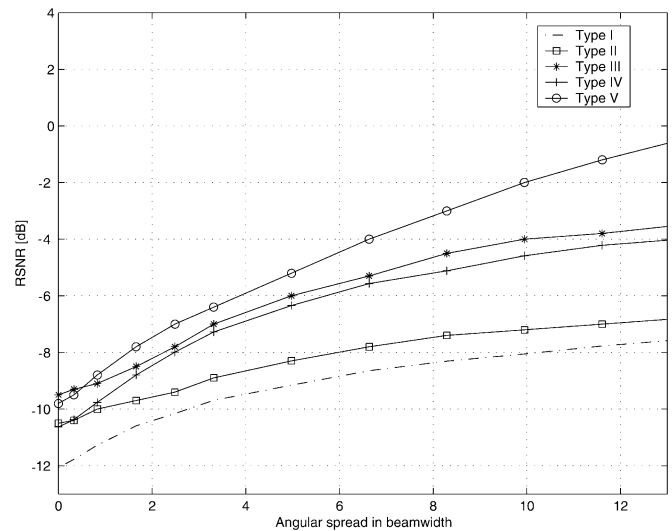


Fig. 14. RSNR versus normalized angular spread for Type I, II, III, IV, and V detectors. The number of measurements is $T = 20$. The target detection probability rate $P_D = 0.8$, and the false alarm rate $P_{FA} = 10^{-3}$.

the detection probability and RSNR for the Type I, II, III, IV, and V detectors with $T = 20$ data snapshots. We observe that the detection performance in this case appears to be quite different than that with a single measurement. With multiple measurements, as the angular spread increases, the detection performance degrades monotonically. This observation suggests that large degrees of freedom, caused either by multiple measurements or by a large angular spread, bring down the detection performance. Nevertheless, the performance of the beamformer detectors degrade faster than that of the GLR detectors. The simulation results in Figs. 13 and 14 demonstrate that the GLRs have better performance than the beamformer detectors as the angular spread increases.

VI. CONCLUSIONS

In this paper, we studied GLR-based detectors for spatially distributed signal sources. The analysis and computer simula-

tion demonstrate that the performance of GLR detectors is better than that of conventional beamformer detectors, which are designed for point sources. The performance difference increases as angular spread increases.

APPENDIX ML ESTIMATES OF $(\hat{\rho}, \hat{\sigma}^2)$

Under H_0 , the only unknown parameter is σ_0^2 . The derivation of its maximum likelihood estimate $\hat{\sigma}_0^2$ is straightforward by maximizing the likelihood function for H_0

$$\begin{aligned} f(\mathbf{X}, H_0) &= [\pi^P |\sigma^2 \mathbf{I}|]^{-T} \exp \left\{ -\frac{1}{\sigma^2} \text{Tr}[\mathbf{X}^H \mathbf{X}] \right\} \\ &= [\pi^P |\sigma^2 \mathbf{I}|]^{-T} \exp \left\{ -\frac{T}{\sigma^2} \text{Tr}[\mathbf{Q}] \right\} \end{aligned} \quad (52)$$

respective to $\hat{\sigma}_0^2$, where sample covariance matrix $\mathbf{Q} = (1/T)\mathbf{X}\mathbf{X}^H$. We obtain $\hat{\sigma}_0^2 = (1/P)\text{Tr}[\mathbf{Q}]$. Substituting back into the PDF under H_0

$$f(\mathbf{X}, \hat{\sigma}_0^2, H_0) = \frac{1}{(e\pi)^{TP}} \left(\frac{P}{\text{Tr}[\mathbf{Q}]} \right)^{TP}. \quad (53)$$

Under H_1 , (ρ, σ^2) are the unknowns. The PDF of \mathbf{X} is

$$f(\mathbf{X}, H_1) = [\pi^P |\mathbf{R}_1|]^{-T} \exp \left\{ -T \text{Tr}[\mathbf{R}_1^{-1} \mathbf{Q}] \right\}. \quad (54)$$

The MLE of σ^2 under H_1 is $\hat{\sigma}_1^2 = (1/P)\text{Tr}[(\rho \mathbf{R}_s + \mathbf{I})^{-1} \mathbf{Q}]$. Inserting it to the likelihood function leads to

$$\begin{aligned} f(\mathbf{X}, H_1, \hat{\sigma}_1^2) &= \frac{1}{(e\pi)^{PT}} \left(\frac{P}{\text{Tr}[(\rho \mathbf{R}_s + \mathbf{I})^{-1} \mathbf{Q}]} \right)^{PT} \\ &\quad \times \frac{1}{|\rho \mathbf{R}_s + \mathbf{I}|^T}. \end{aligned} \quad (55)$$

Partial derivatives of $\ln f(\mathbf{X}, H_1, \hat{\sigma}_1^2)$ with respect to ρ yield the following nonlinear equation:

$$\begin{aligned} \frac{\partial}{\partial \rho} \ln f(\mathbf{X}, H_1, \hat{\sigma}_1^2) &= PT \frac{\text{Tr}[(\rho \mathbf{R}_s + \mathbf{I})^{-1} \mathbf{Q} (\rho \mathbf{R}_s + \mathbf{I})^{-1} \mathbf{R}_s]}{\text{Tr}[(\rho \mathbf{R}_s + \mathbf{I})^{-1} \mathbf{Q}]} \\ &\quad - T \text{Tr}[(\rho \mathbf{R}_s + \mathbf{I})^{-1} \mathbf{R}_s]. \end{aligned} \quad (56)$$

The MLE of $\hat{\rho}$ is the real root of the nonlinear equation $(\partial/\partial \rho) \ln f(\mathbf{X}, H_1, \hat{\sigma}_1^2) = 0$. Solving this equation is equivalent to solving the numerator only, i.e.,

$$\begin{aligned} P \text{Tr}[(\rho \mathbf{R}_s + \mathbf{I})^{-1} \mathbf{Q} (\rho \mathbf{R}_s + \mathbf{I})^{-1} \mathbf{R}_s] \\ - [\text{Tr}(\rho \mathbf{R}_s + \mathbf{I})^{-1} \mathbf{Q}] \text{Tr}[(\rho \mathbf{R}_s + \mathbf{I})^{-1} \mathbf{R}_s] = 0. \end{aligned} \quad (57)$$

Assuming that the subspace \mathbf{R}_s has rank r , the above equation can be rewritten as

$$\begin{aligned} g(\rho) &= P \sum_{i=1}^r \frac{\lambda_i \text{Tr}[\mathbf{P}_{\mathbf{u}_i} \mathbf{Q}]}{(\rho \lambda_i + 1)^2} - \sum_{i=1}^r \frac{\lambda_i}{\rho \lambda_i + 1} \\ &\quad \times \left(\sum_{i=1}^r \frac{\text{Tr}[\mathbf{P}_{\mathbf{u}_i} \mathbf{Q}]}{\rho \lambda_i + 1} + \text{Tr}[\mathbf{P}_{\mathbf{U}_r}^\perp \mathbf{Q}] \right) = 0. \end{aligned} \quad (58)$$

Further simplification indicates that this equation is also a polynomial function of ρ with order $2r - 1$. It is well known that roots of polynomial functions appear in pairs. This real non-negative root $\rho \geq 0$ is the MLE of ρ . If the root $\rho < 0$, we immediately reject H_1 and accept H_0 .

This observation suggests a numerical procedure for computing MLE $\hat{\rho}$ by seeking the real root of polynomial function $g(\rho) = 0$. The search is carried out by a binary search over the range $[0, \rho_0]$, where ρ_0 is a sufficiently large number.

Once the MLE $\hat{\rho}$ is sought, one can construct the compressed likelihood ratio using the above PDFs, with the MLEs in place of the unknown parameters, i.e.,

$$l(\mathbf{X}, \hat{\rho}, \hat{\sigma}_1^2, \hat{\sigma}_0^2) = \left(\frac{\text{Tr}[\mathbf{Q}]}{\text{Tr}(\hat{\rho} \mathbf{R}_s + \mathbf{I})^{-1} \mathbf{Q}} \right)^{PT} \frac{1}{|\hat{\rho} \mathbf{R}_s + \mathbf{I}|^T}. \quad (59)$$

Taking the logarithm of $l(\mathbf{x}; \hat{\rho}, \hat{\sigma}_1^2, \hat{\sigma}_0^2)$, we have

$$L(\mathbf{X}, \hat{\rho}, \hat{\sigma}_1^2, \hat{\sigma}_0^2) = PT \ln \frac{\text{Tr}[\mathbf{Q}]}{\text{Tr}[(\hat{\rho} \mathbf{R}_s + \mathbf{I})^{-1} \mathbf{Q}]} - T \ln |\hat{\rho} \mathbf{R}_s + \mathbf{I}|. \quad (60)$$

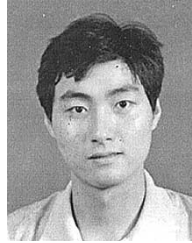
ACKNOWLEDGMENT

The authors would like to thank the anonymous reviewers for their helpful suggestions that considerably improved the quality of this paper.

REFERENCES

- [1] Y. Abramovich, N. Spencer, and A. Gorohov, "Detection-estimation of distributed Gaussian sources," in *Proc. Sensor Array Multichannel Signal Process. Workshop*, 2002, pp. 513–517.
- [2] F. Adachi, M. T. Feeney, A. G. Williamson, and J. D. Parsons, "Crosscorrelation between the envelopes of 900 MHz signals received at a mobile radio base station site," *Proc. Inst. Elect. Eng. F*, vol. 133, no. 6, pp. 506–512, Oct. 1991.
- [3] T. W. Anderson, *An Introduction to Multivariate Statistical Analysis*, Second ed. New York: Wiley, 1984.
- [4] O. Besson and P. Stoica, "Decoupled estimation of DOA and angular spread for a spatially distributed source," *IEEE Trans. Signal Processing*, vol. 48, pp. 1872–1882, July 2000.
- [5] G. E. P. Box, "Some theorems on quadratic forms applied in the study of analysis of variance problems, I. Effect of inequality of variance in the one-way classification," *Ann. Math. Statist.*, vol. 25, no. 2, pp. 290–302, June 1954.
- [6] H. Cox, "Multi-rate adaptive beamforming (MRABF)," in *Proc. IEEE Sensor Array Multichannel Signal Process. Workshop*, 2000, pp. 308–309.
- [7] P. Eggers, "Angular propagation descriptions relevant for base station adaptive antenna operations," *Wireless Pers. Commun.*, vol. 11, no. 1, pp. 3–29, Oct. 1999.
- [8] B. Friedlander and Y. Jin, "Adaptive array processing for distributed sources," in *Proc. 35th Asilomar Conf. Signals, Syst., Comput.*, Nov. 2001.
- [9] C. W. Helstrom, *Statistical Theory of Signal Detection*, second ed. New York: Pergamon, 1968.
- [10] F. Ikegami and S. Yoshida, "Analysis of multipath propagation structure in urban mobile radio environments," *IEEE Trans. Antennas Propagat.*, vol. AP-28, pp. 531–537, July 1980.
- [11] H. B. Lee, "Eigenvalues and eigenvectors of covariance matrices for signals closely spaced in frequency," *IEEE Trans. Signal Processing*, vol. 40, pp. 2518–2535, Oct. 1992.
- [12] W. C.-Y. Lee, "Finding the approximate angular probability density function of wave arrival by using a directional antenna," *IEEE Trans. Antennas Propagat.*, vol. AP-21, pp. 328–334, May 1973.
- [13] E. Lehmann, *Testing Statistical Hypotheses*, 2nd ed. New York: Wiley-Interscience, 1986, pp. 284–286.

- [14] M. T. Ma, *Theory and Application of Antenna Arrays*. New York: Wiley, 1974.
- [15] L. T. McWhorter and L. L. Scharf, "Matched subspace detectors for stochastic signals," unpublished, 2001.
- [16] B. Ottersten, M. Viberg, P. Stoica, and A. Nehorai, "Exact and large sample maximum likelihood techniques for parameter estimation and detection in array processing," in *Radar Array Processing*, S. Haykin, J. Litva, and T. Shepherd, Eds. New York: Springer-Verlag, 1992.
- [17] K. I. Pedersen, P. E. Mogensen, and B. H. Fleury, "Power azimuth spectrum in outdoor environments," *Electron. Lett.*, vol. 33, pp. 1583–1584, Aug. 1997.
- [18] R. S. Raghavan, N. Pulsone, and D. J. McLaughlin, "Performance of the GLRT for adaptive vector subspace detection," *IEEE Trans. Aerosp. Electron. Syst.*, vol. 32, pp. 1473–1487, Oct. 1996.
- [19] R. Raich, J. Goldberg, and H. Messer, "Bearing estimation for a distributed source: Modeling, inherent accuracy limitations and algorithms," *IEEE Trans. Signal Processing*, vol. 48, pp. 429–441, Feb. 2000.
- [20] J. Salz and J. H. Winters, "Effect of fading correlation on adaptive arrays in digital mobile radio," *IEEE Trans. Veh. Technol.*, vol. 43, pp. 1049–1057, Nov. 1994.
- [21] L. L. Scharf and B. Friedlander, "Matched subspace detection," *IEEE Trans. Signal Processing*, vol. 42, pp. 2146–2157, Aug. 1994.
- [22] L. L. Scharf, *Statistical Signal Processing*. Reading, MA: Addison-Wesley, 1991.
- [23] S. Valaee, B. Champagne, and P. Kabal, "Parametric localization of distributed sources," *IEEE Trans. Signal Processing*, vol. 43, pp. 2144–2153, Sept. 1995.



Yuanwei Jin (S'99–M'04) received the M.S. degree in mathematics from East China Normal University, Shanghai, China, in 1996 and the Ph.D. degree in electrical engineering from the University of California, Davis, in 2003.

He was a lecturer with the Department of Mathematics, Nanjing University of Science and Technology, Nanjing, China. In the summer of 1999, he was with Sensys Instrument Corporation, Santa Clara, CA. His research interests are in signal processing, array processing, estimation, and

detection.

Dr. Jin received the Earle C. Anthony Fellowship from UC Davis from 1997 to 1999.



Benjamin Friedlander (S'74–M'76–SM'82–F'87) received the B.Sc. and the M.Sc. degrees in electrical engineering from the Technion—Israel Institute of Technology, Haifa, Israel, in 1968 and 1972, respectively, and the Ph.D. degree in electrical engineering and the M.Sc. degree in statistics from Stanford University, Stanford, CA, in 1976.

From 1976 to 1985, he was with Systems Control Technology, Inc., Palo Alto, CA. From November 1985 to July 1988, he was with Saxpy Computer Corporation, Sunnyvale, CA. From 1989 to 1999,

he was at the University of California, Davis. Currently, he is a professor of electrical engineering at the University of California, Santa Cruz.

Dr. Friedlander received the 1983 ASSP Senior Award, the 1985 Award for the Best Paper of the Year from the European Association for Signal Processing (EURASIP), the 1989 Technical Achievement Award of the IEEE Signal Processing Society, and the IEEE Third Millennium Medal.